nearest neighbors over that resulting from the superposition of atomic charge. We may define it by

$$Q=\int[\rho(\mathbf{r})-\rho_{at}(\mathbf{r})]\,d^3r,$$

where the integration is limited to the region about **M** in which the integrand is positive. We estimate $Q\approx 0.03$ a.u.

One can also estimate Q from the Fourier coefficients of the self-consistent potential calculated in *I*. One of these, $F(\bar{1}11)$, differs appreciably from the free-atom value and also leads to $Q\approx 0.03$ a.u. Thus, as anticipated in I, the bonding charge is largely represented by this Fourier coefficient.

According to Phillips,[2] the volume occupied by the bonding charges should be very small. We estimate the (total) volume occupied by the three bonding charges in the primitive cell to be about 4% of the volume of that cell.

The ionic binding energy per atom from this charge is ≈ 0.002 a.u., negligible compared with the experimental value of 0.11 a.u. Actually, on an atomic picture, most of the binding energy comes simply from the (nonbonding) overlap of the spherical charge distributions of nearest neighbors. Using HF wave functions,[10] we have calculated this energy to be 0.30 a.u.; thus, the repulsive terms must contribute at least -0.2 a.u. to the binding energy.

ACKNOWLEDGMENTS

We wish to thank C. S. Barrett, M. H. Cohen, L. M. Falicov, W. Goldburg, D. Haftmeister, F. Keffer, I. Lowe, D. Schiferl, and P. Stone for useful conversations.

PHYSICAL REVIEW B VOLUME 1, NUMBER 2 15 JANUARY 1970

Resistivity of Iron as a Function of Magnetization and Stress*

P. W. Shumate, Jr.,† R. V. Coleman, and R. C. Fivaz
Department of Physics, University of Virginia, Charlottesville, Virginia 22903
(Received 2 June 1969; revised manuscript received 6 October 1969)

The resistance and magnetoresistance of iron single crystals have been measured as a function of stress at liquid-helium temperatures. For measuring currents above some critical value, a large transition in the resistance of the sample is observed, and the critical current for this transition is a function of both the applied longitudinal magnetic field and the applied axial stress. The results have been interpreted in terms of inverse-magnetostriction and domain-reorientation effects involving the self-field of the current. We have developed a model for the ⟨100⟩-axial crystals based on a sheath-core configuration with spins perpendicular and parallel to the current in the sheath and core, respectively. Under favorable conditions the formation of the sheath-core configuration simulates the behavior of thermodynamical variables in a first-order phase transition. The analysis of the model can be used to predict the observed resistance transition quite accurately and can also be used to obtain a value of the saturation magnetostriction constant λ_{100}. The value obtained is $\lambda_{100}=(25.0\pm1.0)\times10^{-6}$, which is in reasonable agreement with other measurements. Results of stress experiments on ⟨111⟩-axial crystals are consistent with a negative value of λ_{111}, but indicate that the field and current-induced resistance transitions are more complex than those in the ⟨100⟩-axial crystals. Discussion of possible mechanisms is included.

I. INTRODUCTION

In previous papers,[1–3] we have reported results of electrical-resistance measurements in iron single crystals, particularly in the low-temperature range extending to 1°K. A striking characteristic has been large negative magnetoresistance behavior observed in the liquid-helium temperature range. In the case of ⟨100⟩ specimens, this behavior was shown to be primarily induced by the self-field of the measuring current and was interpreted as a reverse galvanomagnetic effect[3] connected with the formation of various domain configurations.

In this paper, we report on a series of results obtained by applying uniaxial stress to the crystal and measuring resistance as a function of stress, magnetic field, and measuring current. The use of uniaxial stress as an additional variable has allowed a precise control of the magnetic state of the crystal through inverse magnetostriction. This has allowed us to make a more complete interpretation of the resistance and magnetoresistance behavior in the helium temperature range, and has also provided a fairly accurate value of the magnetostriction constant for iron at helium temperatures.

* Work supported in part by the U. S. Atomic Energy Commission and the U. S. Army Research Office, Durham, N. C.
† Present address: Bell Telephone Laboratories, Murray Hill, N. J.
[1] A. Isin and R. V. Coleman, Phys. Rev. **142**, 372 (1966).
[2] R. V. Coleman and A. Isin, J. Appl. Phys. **37**, 1028 (1966).
[3] G. R. Taylor, A. Isin, and R. V. Coleman, Phys. Rev. **165**, 621 (1968).

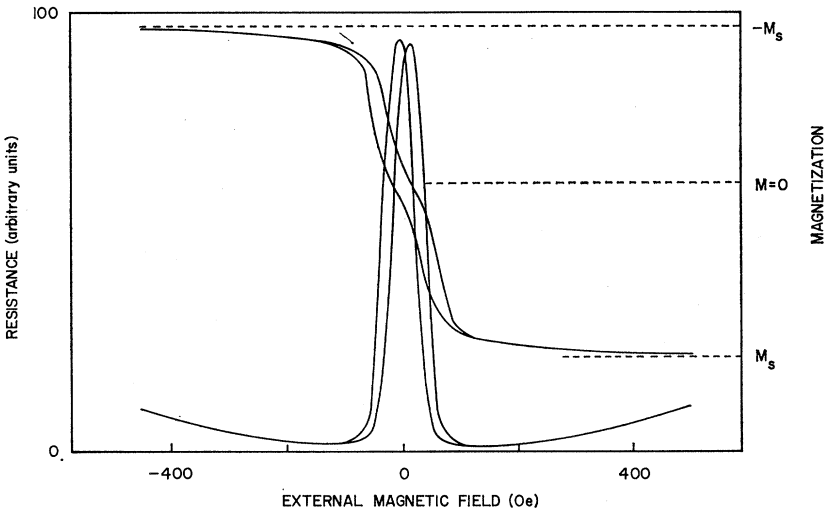

FIG. 1. Magnetoresistance (lower curve) and magnetization (upper curve) of ⟨100⟩-axial iron crystals as a function of the magnetic field.

The iron crystals used in this work were single-crystal whiskers grown by the reduction of ferrous chloride.[4] Such crystals, because of their high purity and high geometric perfection, show a large region of elastic behavior.[5] More will be said regarding the purity characterization in Sec. II.

II. EXPERIMENTAL RESULTS

A. Magnetoresistance and Magnetization

The low-field longitudinal magnetoresistance of iron single crystals has been observed to follow the magnetization rather closely when a reasonably high measuring current is used, ~1–3 A for the present specimens. The flux-closed or $\mathbf{M}=0$ state corresponds to a maximum value of resistance while a minimum value of resistance is observed for the nearly saturated state $\mathbf{M}\sim\mathbf{M}_s$. Curves of resistance and magnetization measured simultaneously at 4.2°K are shown in Figs. 1 and 2 for a ⟨100⟩- and ⟨111⟩-axial iron crystal, respectively. The resistance shows a hysteresis with a width corresponding to the coercivity observed in the magnetization curve. The hysteresis observed here begins at temperatures just below 77°K and increases down to the lowest temperatures measured, ~0.3°K. The ⟨111⟩-axial crystal shows two magnetization regions corresponding to different slopes on the **M**-**H** plot. The initial steep slope corresponds to magnetization by domain boundary motion while the second lower-slope region corresponds to magnetization by coherent spin rotation from a ⟨100⟩ to a ⟨111⟩ direction. These two regions are also easily identified in the R-versus-**H** plot. In the ⟨100⟩ case, only

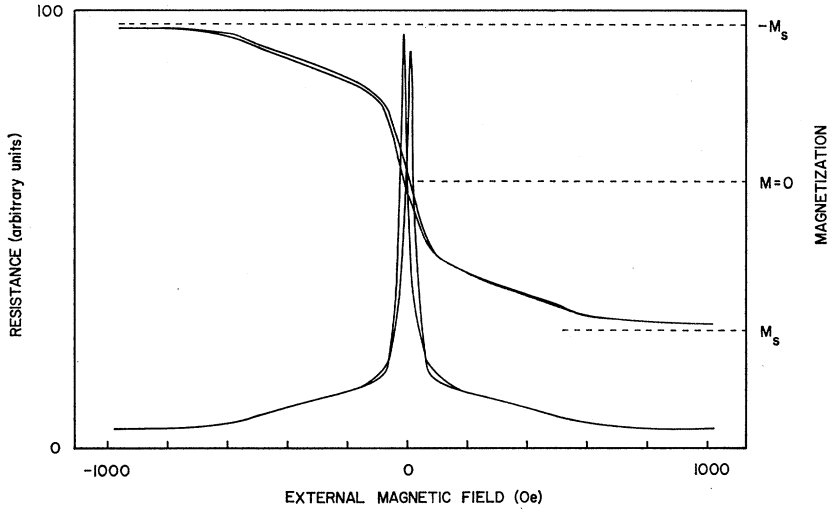

FIG. 2. Magnetoresistance (lower curve) and magnetization (upper curve) of ⟨111⟩-axial iron crystals as a function of the magnetic field.

[4] S. S. Brenner, Acta Met. **4**, 62 (1956).
[5] S. S. Brenner, in *Growth and Perfection of Crystals*, edited by R. H. Doremus *et al.* (John Wiley & Sons, Inc., New York, 1958), p. 157.

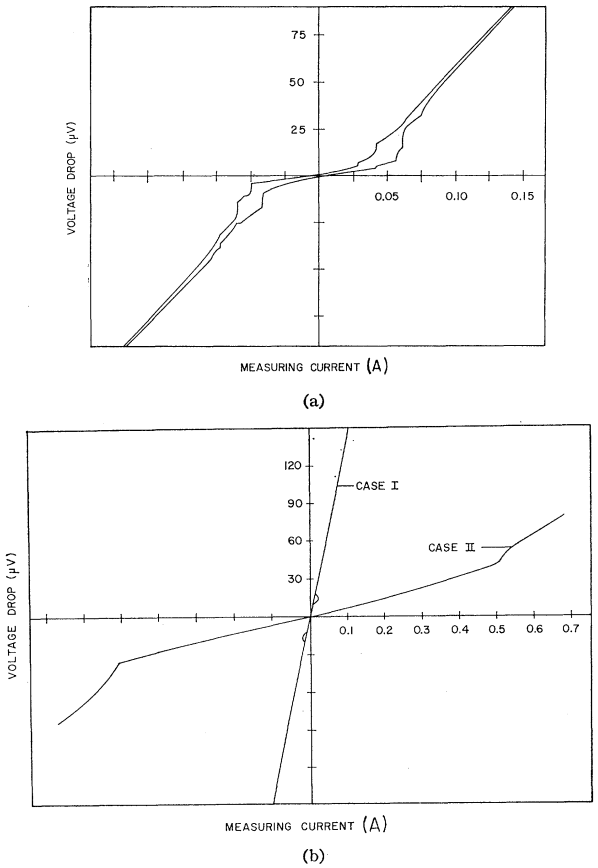

FIG. 3. (a) Current-voltage characteristic of unstressed ⟨100⟩-axial iron crystals. (b) Current-voltage characteristic of unstressed ⟨111⟩-axial iron crystals.

the region corresponding to magnetization by domain-wall motion is seen since the applied field is in a ⟨100⟩ easy direction.

If the measuring current is reduced to a few milliamperes, then the R-versus-$\mathbf{H}$ curves for the ⟨100⟩-axial crystals no longer show any evidence of the region corresponding to magnetization by domain-wall motion, and the resistance is independent of magnetization. This behavior is equivalent to saying that in the $\mathbf{M}=0$ state the resistance shows a substantial dependence on the measuring current, while the nearly saturated state $\mathbf{M}\sim\mathbf{M}_s$ obeys Ohm's law. The extra magnetoresistance induced by the measuring current at the $\mathbf{M}=0$ state can also be observed by recording the voltage drop as a function of measuring current. Such a recording is shown in Fig. 3(a), and the transition from lower to higher slope represents the resistance transition induced by increasing the measuring current. Both increasing and decreasing current curves have been recorded and hysteresis is observed in the region of the transition, further indicating that domain rearrangement takes place during the current-induced resistance transition in ⟨100⟩-axial specimens.

In the case of ⟨111⟩-axial crystals, the resistance decrease corresponding to coherent spin rotation is essentially independent of current. The resistance peak at $\mathbf{M}=0$ shows some current dependence, but it is not induced entirely by the current as is the case for ⟨100⟩-axial crystals. The amount of current-induced resistance at $\mathbf{M}=0$ is observed to vary from specimen to specimen and voltage-versus-current curves for two ⟨111⟩-axial specimens are shown in Fig. 3(b). One crystal in Fig. 3(b) shows a substantial current dependence and resistance transition while the other shows practically none. Indications are that the perfect ⟨111⟩ crystals show a resistance peak at $\mathbf{M}\simeq 0$ which is entirely independent of current and that those that show some current dependence are probably less perfect. This peak is of the same magnitude as the current-induced peak observed in ⟨100⟩ specimens. This point will be discussed further in Sec. III, but at present the ⟨100⟩-axial crystal behavior is more fully understood and the stress results and analysis provide a complete picture of the magnetoresistance behavior in ⟨100⟩ specimens.

Since the residual-resistance ratio RRR,R(300°K)/R(4.2°K), is frequently used to characterize the purity of a metallic specimen, this anomalous negative-

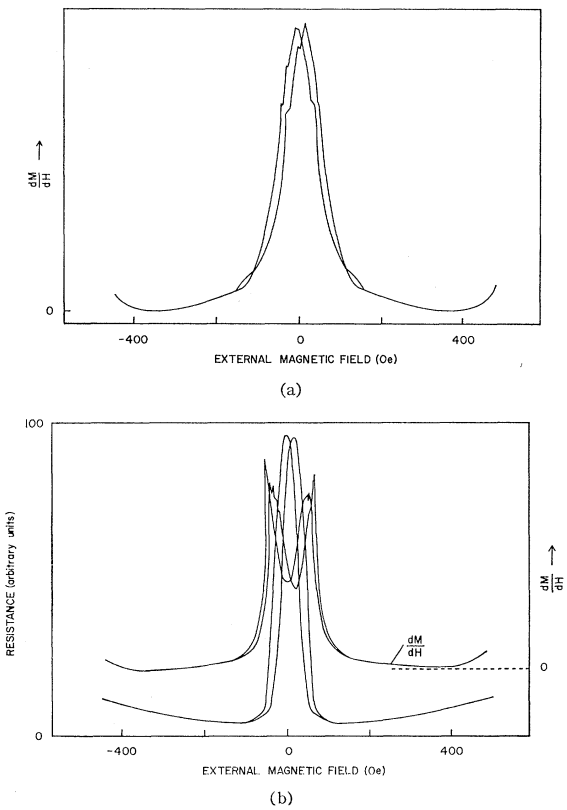

FIG. 4. (a) Derivative of the M-H curve for ⟨100⟩-axial iron crystals as a function of the magnetic field, at zero measuring current. (b) Derivative of the M-H curve for ⟨100⟩-axial iron crystals as a function of magnetic field, at a measuring current of 2 A. The lower curve is the corresponding magnetoresistance.

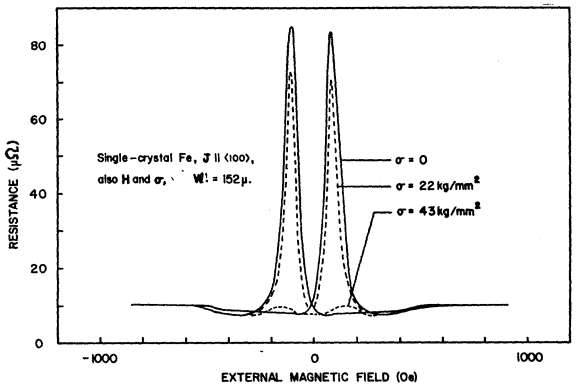

FIG. 5. Magnetoresistance curves for a ⟨100⟩-axial iron crystal for tensile stresses of 0, 22, and 43 kg/mm².

resistance behavior near $\mathbf{H}=0$ with its associated wide range of values causes difficulties. With no external field applied, the maximum value of the RRR is frequently no higher than 250–300. However, with a field applied which causes partial saturation of the crystal magnetization, values of the RRR up to 8000 have been measured by this laboratory. Typical values of the RRR thus measured are in the range of 1000–2000. Other investigators[6] have attempted to arrive at a meaningful RRR by numerical extrapolation of $R(\mathbf{B})$ to $\mathbf{B}=0$. The high values of the RRR indicate further the high purity of the crystals used here.

The effects of the measuring current have also been studied by recording the derivative of magnetization with respect to $\mathbf{H}$ at zero current and at 2–3 A. As shown in Figs. 4(a) and 4(b), the self-field of the measuring current in the ⟨100⟩ specimens retards the development of magnetization at $\mathbf{H}=0$. Figure 4(a) shows dM/dH versus $\mathbf{H}$ with a maximum at $\mathbf{H}=0$ for zero current while Fig. 4(b) shows dM/dH versus $\mathbf{H}$ for a measuring current of 2 A. The corresponding R-versus-$\mathbf{H}$ curve is also included in Fig. 4(b). The maximum in dM/dH is clearly shifted from $\mathbf{H}=0$ and corresponds to the most rapid decrease in resistance with $\mathbf{H}$. Similar effects at $\mathbf{H}=0$ are observed for the ⟨111⟩ crystals, and in both cases a substantial effect of the measuring current on magnetization development is observed.

The magnetoresistance observations reported above have been generally understood in terms of the reverse galvanomagnetic effect[3] by the present authors as well as a number of other investigators.[7,8] Domain-wall scattering has also been suggested as a possible mechanism for explaining some of the observations.[9,10]

The reverse galvanomagnetic model is based simply on the comparison of transverse with longitudinal magnetoresistance contributions for various domain configurations in which the spin direction is perpendicular or parallel to the current. The conduction electrons are assumed to feel the internal field of ~22 kG within each domain and the resistance therefore has a standard magnetoresistance term due to the Lorentz force. Our experiments can be interpreted on ⟨100⟩-axial crystals in terms of the angles between the current axis and spin directions which are consistent with the observed behavior. However, other models, such as those showing Fermi-surface topology changes induced by changes in the spin direction relative to current axis, might also be consistent with the experimental results. In fact, the data on ⟨111⟩-axial specimens which show a current-independent resistance peak at the $\mathbf{M}=0$ state appear to require some mechanism in addition to the reverse galvanomagnetic effect, although the ⟨100⟩ data are completely consistent with the reverse galvanomagnetic argument.

In the present group of experiments, we find that axial stress has a large effect on the helium-temperature magnetoresistance and that analysis of the results has added considerable detail and understanding to the problem. In Sec. II B, we report the stress results for both the ⟨100⟩- and ⟨111⟩-axial specimens.

B. Uniaxial Stress Applied to ⟨100⟩-Axial Whiskers

Elastic stresses up to 50 kg/mm² have been applied to ⟨100⟩-axial whiskers and the resistance as a function of magnetic field and measuring current has been recorded. Examples of the R-versus-$\mathbf{H}$ curves for a measuring current of 2 A are shown in Fig. 5. Curves are shown for applied stresses of 0, 22, and 43 kg/mm². For this measuring current, it is clear that the magnetoresistance associated with the region of domain-

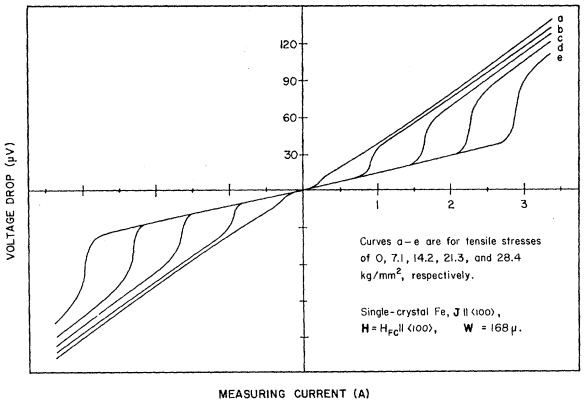

FIG. 6. Typical current-voltage characteristics of a ⟨100⟩-axial iron crystal for various stresses.

[6] A. I. Schlindler and B. C. LaRoy, J. Appl. Phys. **37**, 3610 (1966).
[7] Eiji Tatsumoto, Phys. Rev. **109**, 658 (1958).
[8] L. Berger and A. R. deVroomen, J. Appl. Phys. **36**, 2777 (1965).
[9] A. I. Sudovtsov and E. E. Semenenko, Zh. Eksperim. i Teor. Fiz. **35**, 305 (1958) [English transl.: Soviet Phys.—JETP **8**, 211 (1959)].
[10] E. E. Semenenko and A. I. Sudovtsov, Zh. Eksperim. i Teor. Fiz. **47**, 486 (1964) [English transl.: Soviet Phys.—JETP **20**, 323 (1965)].

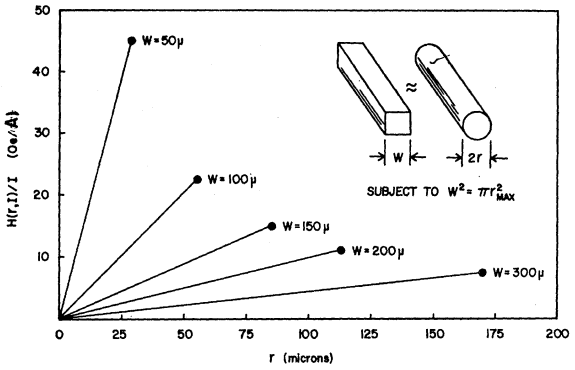

FIG. 7. Variation of the self-field of the measuring current from the center of the crystal to the surface, approximated from the inset diagram.

boundary motion can be completely quenched by applying sufficient stress. Increasing the measuring current will, however, cause a corresponding increase in the stress required to quench the magnetoresistance. An alternative experiment which shows essentially the same basic behavior consists of measuring the voltage drop across the specimen as a function of measuring current for a number of constant applied-stress values. A group of such curves is shown in Fig. 6. The transition region in these curves again corresponds to the region where the magnetoresistance is rising strongly with increase of current (strong deviation from Ohm's law). For higher applied stresses the transition region shifts to successively higher measuring-current values. In the case of ⟨100⟩-axial specimens, the curves above the transition converge toward the same straight line. Since the self-field associated with the measuring current is an important parameter in these results, we have calculated the value at the surface of the whisker when the transition just begins by assuming a uniform current in a specimen of circular cross section equal to that of the specimen. The appropriate values corresponding to the curves of Fig. 6 can be estimated from Fig. 7, which shows self-field of current in Oe per ampere as a function of radial distance for whiskers of various diameters.

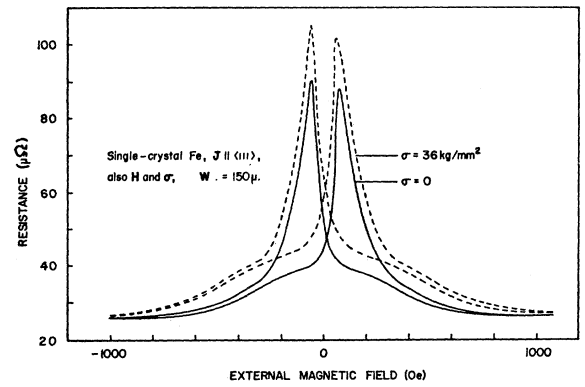

FIG. 8. Magnetoresistance curves for a ⟨111⟩-axial iron crystal for tensile stresses of 0 and 36 kg/mm².

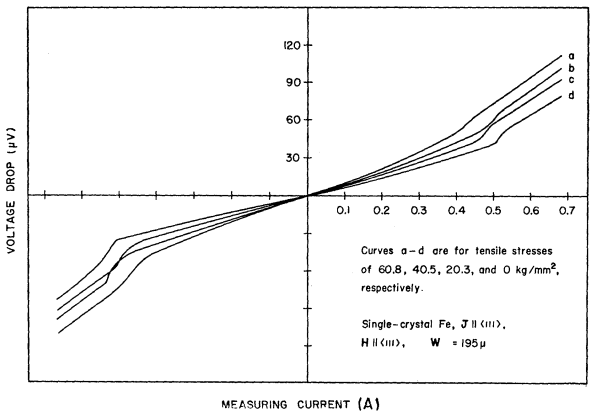

FIG. 9. Typical current-voltage characteristics of ⟨111⟩-axial iron crystal for various stresses.

C. Uniaxial Stress Applied to ⟨111⟩-Axial Whiskers

In the case of stress applied to the ⟨111⟩-axial specimens, the R-versus-$\mathbf{H}$ curves are modified as shown in Fig. 8 for a measuring current of 2 A. The application of stress causes an increase of the magnetoresistance for all regions of the R-versus-$\mathbf{H}$ curve below the field value corresponding to saturation (see Fig. 2). This can be seen in the voltage-drop–versus–$\mathbf{I}$ curves under constant stress, which are shown in Fig. 9 for a ⟨111⟩-axial specimen. The transition corresponding to the deviation from Ohm's law is also observed in this specimen, and in this case it is shifted to lower critical-current values by the application of stress. The high-current region following the transition is also appreciably affected by the stress, with the result that higher stress values produce higher resistance and the curves do not converge, as was the case for the ⟨100⟩ specimens. Both the ⟨100⟩ and the ⟨111⟩ results can be discussed in terms of inverse magnetostriction effects and this will be covered in Sec. III.

D. Domain Configuration from Powder Patterns

In order to obtain information on the effect of the measuring current on the domain configuration, we have carried out a number of experiments at room temperature using the standard Bitter technique to observe the domain walls.[11,12] The results are, of course, necessarily valid only at room temperature, but we see no reason to expect substantial changes in domain structure at liquid-helium temperatures. We have simply observed the changes in surface-domain configuration as we apply axial currents to the specimen. For the ⟨100⟩ specimens, we observe a single central wall as shown in Fig. 10(a) when no current is flowing in the specimen. When a current sufficient to saturate the resistance at helium

[11] G. G. Scott and R. V. Coleman, J. Appl. Phys. 28, 1512 (1957).

[12] G. Lidgard and W. D. Corner, IEEE Trans. Magnetics 2, 499 (1966).

temperature and $\mathbf{M}=0$ is switched on, the magnetite begins to disperse and after 30 sec no walls are observed on the specimen surface. Figures 10(b) and 10(c) show the pattern sequence when the current is just switched on and after 30 sec. Switching off the current restores the wall as seen in Fig. 10(d). The three-dimensional domain-structure sequence developed for the ⟨100⟩ specimen in Ref. 3 and shown in Fig. 11 is completely consistent with the above domain-wall observations.

The ⟨111⟩-axial specimens show no domain walls on the ⟨110⟩ surfaces either with currents on or off. The current-off state corresponds to the three-dimensional six-domain structure shown in Fig. 12(a) and the present experiments are not able to pick up any modification of surface structure due to the current. This indicates that any modifications leave the surface intersections of walls along the corners of the whisker as they were in the current-off state. This is not unreasonable since the initial structure is already partially solenoidal with respect to the self-field of the current, and one would not expect such dramatic changes to occur as are observed for the ⟨100⟩ case. Unfortunately, however, this result sheds no light on the source of the magnetoresistance peak at $\mathbf{M}=0$ observed for ⟨111⟩-axial specimens.

III. DISCUSSION AND INTERPRETATION

As noted in previous papers, the data on ⟨100⟩ specimens appear to be subject to a more detailed interpretation, and this continues to be the case in the present experiments. The stress effects on the ⟨100⟩ magnetoresistance are consistent with all previous data, and we are able to develop a detailed model based on inverse magnetostriction and self-field effects of the current. In addition, this model allows us to make a fairly accurate determination of the magnetostriction constant λ_{100} at helium temperature. The stress effects for ⟨111⟩-axial crystals have cleared up a number of points concerning the source of ⟨111⟩ magnetoresistance changes, but a detailed model of the magnetoresistance behavior, particularly the magnetoresistance peak at $\mathbf{M}=0$, is still lacking.

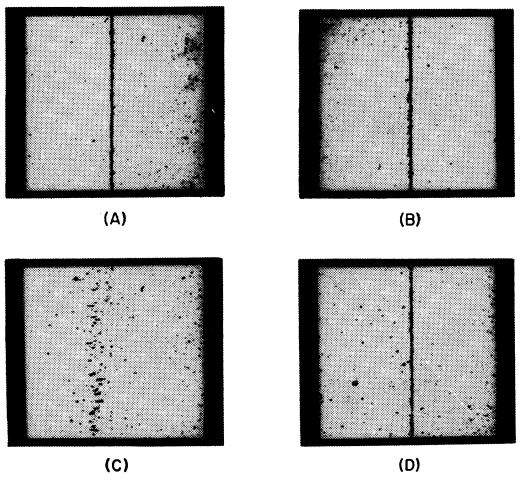

FIG. 10. Bitter-pattern photographs showing the annihilation and reformation of a longitudinal 180° Bloch wall caused by varying the longitudinal measuring current. (A) zero current, (B) and (C) current on, (D) zero current.

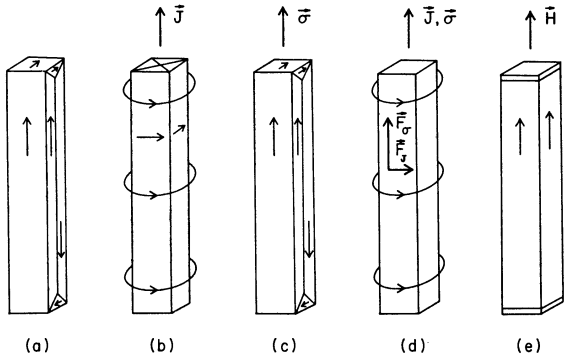

FIG. 11. Proposed domain structures (a)–(e) for various combinations of currents, stresses, and magnetic fields.

A. Inverse Magnetostriction and Current Self-Field

The quenching of the current-induced magnetoresistance in ⟨100⟩-axial specimens by tensile stress suggests that the self-field of the current and inverse magnetostriction have counteracting effects on the spin configuration and resulting domain structure of the specimen. In the presence of stress, the resistance transition will be observed to occur above some critical current which is just sufficient to cancel the inverse magnetostriction effect. We can obtain a quantitative expression for the critical current by writing an equilibrium energy-balance expression based on models for the two processes. We will first discuss inverse magnetostriction and then self-field effects, followed by a comparison of the resulting equations with the experimental data.

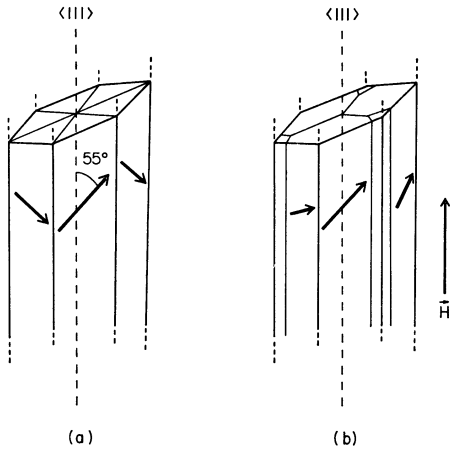

FIG. 12. Domain structure of (a) a demagnetized and (b) a partially magnetized ⟨111⟩-axial iron crystal.

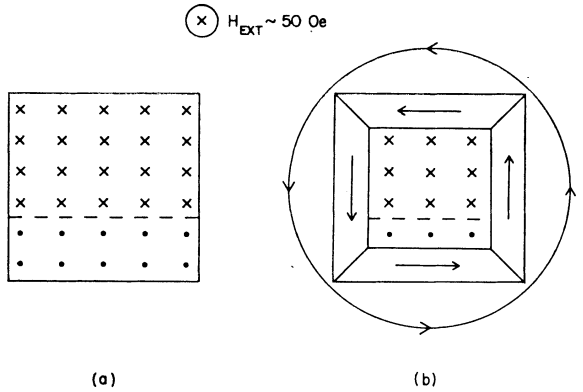

FIG. 13. (a) End-view drawing (not showing demagnetizing effects) of a ⟨100⟩-axial iron crystal. The implied displacement of the 180° wall allows for partial magnetization, and (b) shows the formation of the proposed domain sheath.

Magnetostriction in iron has been studied by a number of authors[13–15] and the saturation-magnetostriction constants have been measured as a function of temperature. The saturation-magnetostriction constant is a measure of the length change which occurs when a ferromagnetic material is magnetized in a given direction. The magnetostriction saturates when the decrease in anisotropy energy caused by the length change is balanced by the increase in the elastic energy of the lattice. If the anisotropy energy of the strained lattice is expressed as a Taylor series expansion in the strains, e_{ij}, it can be written as

$$E_A=(E_A)_{\text{unstrained}}+\sum_{i<j}\left(\frac{\partial E_A}{\partial e_{ij}}\right)_0 e_{ij}$$

$$=(E_A)_{\text{unstrained}}+E_{\text{ME}}, \qquad (1)$$

where E_{ME} is the magnetoelastic energy. The saturation magnetostriction will then be determined by minimizing the total energy given by the expression

$$E_{\text{TOT}}=(E_A)_{\text{unstrained}}+E_{\text{ME}}+\tfrac{1}{2}\mathbf{e}\cdot\mathbf{C}\cdot\mathbf{e}, \qquad (2)$$

where $\mathbf{C}$ is the tensor containing the ordinary elastic moduli.

The inverse of this process is occurring in the present experiments; for the ⟨100⟩ case with positive magnetostriction, a stress applied parallel to the [100] direction will cause the spin direction to align parallel or antiparallel to the stress. The magnetoelastic energy E_{ME} for the [100] direction will be $-\frac{3}{2}\lambda_{100}\sigma$ relative to the two other easy directions of magnetization, [010] and [001]. On the other hand, stress applied parallel to a ⟨111⟩ direction would be expected to turn the spin direction away from the ⟨111⟩ direction because of the negative sign of λ_{111}. The stress therefore provides a mechanism which will rotate the spin direction relative to the axis of the specimen.

The self-field of the current can also be effective in rotating the spin direction by influencing the dipole energy of the spin. In the case of the ⟨100⟩-axial specimens, the self-field will tend to align spins perpendicular to the axis in order to reduce the dipole energy of the spins in the self-field. This will also tend to occur in the ⟨111⟩ case, but will require much higher currents for significant rotation, since no easy directions exist perpendicular to ⟨111⟩ and any reduction in dipole energy will have to overcome the large increase in anisotropy energy required to rotate the spin out of an easy direction. For the $\mathbf{M}\simeq 0$ state, any spin rotation will be accomplished by domain reorientation and growth and some model of this process is required in order to make detailed calculations.

B. Model for ⟨100⟩ and Determination of λ_{100}

In the case of the unstressed ⟨100⟩ crystals, the domain configuration consists of two domains with spins parallel and antiparallel to the axis. As the measuring current is increased, the solenoidal field has a maximum value near the surface and one would expect domains with spins perpendicular to the axis to form near the outer radius first. In fact, the simplest and probably the most accurate model would be a sheath structure such as that schematically pictured in Fig. 13. This is also completely consistent with the powder-pattern evidence referred to in Fig. 10. After once forming this sheath, further increase in current will cause the sheath to propagate in toward the center of the whisker. If one also assumes that for spin perpendicular to the current the resistance is much higher than for spin parallel to the current, then the resistance transition can be identified with the sheath formation and propagation. In fact, the high resistance of the sheath will cause an immediate rearrangement of current with more of it flowing in the central low-resistance core. This, in turn, will increase the field near the center and cause the sheath to propagate further in: This sheath formation mechanism which tends to pinch the current into a small central core if $\rho_T \gg \rho_L$ involves a positive feedback leading to an unstable state. If, for example, the sheath is assumed to carry no current, then its magnetic energy increases linearly with its thickness so that the pressure on the sheath-core interface increases without limit inversely as the core radius. This results in the disappearance of the inner core in contradiction to the assumption that it was carrying all of the current. Therefore, in the real sample with a finite resistance ratio between core and sheath an optimum balance exists between the energy gained by increasing the volume of the sheath and the energy lost by decreasing the self-field as more of the current is forced to flow in the sheath.

[13] R. Gersdorf, thesis, University of Amsterdam, 1961 (unpublished).
[14] Eiji Tatsumoto and Tetsuhiko Okamuto, J. Phys. Soc. Japan **14**, 1588 (1959).
[15] G. M. Williams and A. S. Pavlovic, J. Appl. Phys. **39**, 571 (1968).

Applied external fields such as longitudinal magnetic fields or axial stress will lower the energy of the core and the balance will change with a consequent change in the specimen resistance. Detailed analysis of these shifts in the presence of external fields shows that under favorable conditions they are discontinuous and actually simulate the behavior of thermodynamical variables in a first-order phase transition. The observed resistance transitions in the presence of applied stress do in fact appear abrupt and examples are shown in Fig. 14. In the following paragraphs, we outline the analysis showing the conditions for a discontinuous resistance transition in the presence of a longitudinal magnetic field and then extend it to include the presence of an applied axial stress.

For simplicity, we consider first the reverse galvanomagnetic effect caused by the current in a completely cylindrical geometry. Consider a long cylinder of radius w carrying a current **I**. A Bloch wall separates the inner core of radius, a, where the magnetization is axial, from the outer sheath where the magnetization is solenoidal. If the ratio of the longitudinal to the transverse resistivity is denoted by $\kappa=(\rho_L)/(\rho_T)<1$, then the ratio R of the measured cylinder resistance to the core resistance is given by

$$R(y)=1/[\kappa+(1-\kappa)y^2], \tag{3}$$

where $y=a/w$.

The self-field of the current is a maximum at the sheath-core interface and the field in the sheath as a function of the radius r is given by

$$H(r)=(I/2\pi r)[\kappa r^2+(1-\kappa)a^2]/[\kappa w^2+(1-\kappa)a^2]. \tag{4}$$

The magnetic energy per unit length of sheath is given by

$$E(A)=-\int MH(r)\,d^3r=-IMwG(y), \tag{5}$$

where

$$G(y)=[\tfrac{1}{3}\kappa+(1-\kappa)y^2-(1-\tfrac{1}{3}\kappa)y^3]R(y). \tag{6}$$

As shown in Fig. 15, $G(y)$ has a minimum for $a=a_m$ and the corresponding energy minimum determines the spontaneous arrangement of the spins in the current carrying cylinder in the absence of any other force acting on the Bloch wall. The resistance of the sample at the energy minimum will be $R_m=R(y=a_m)$. The value of y for the energy minimum is given by the single real root of the cubic equation obtained from the zero derivative condition and given below:

$$\frac{dG(y)}{dy}=F(y)=0=(1-\kappa)(1-\tfrac{1}{3}\kappa)y^3 -\kappa[\tfrac{4}{3}(1-\kappa)-3(1-\kappa)y]. \tag{7}$$

It is to be noted that, unless κ is close to unity, y at the minimum always has a finite value and therefore a central core of longitudinal magnetization will be present independent of the intensity of the current.

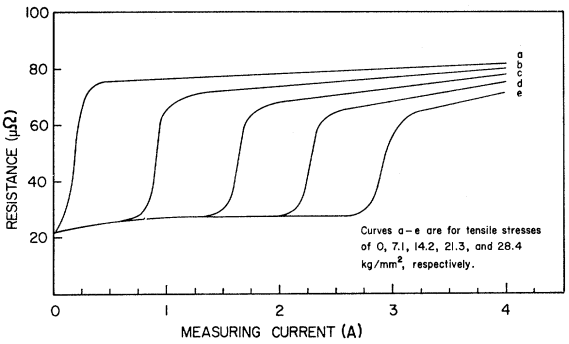

FIG. 14. Resistance as a function of current for a ⟨100⟩-axial iron crystal for various values of stress.

When a longitudinal magnetic field **H** is applied to the specimen, the magnetic energy is lowered by $-\pi HMw^2$ when no sheath is present and by $-\pi HMa^2$ when a sheath of thickness $(w-a)$ is present. Thus, when a sheath is present its energy $E(a)$ must at least balance the difference in energy $HM(w^2-a^2)$. The net balance is given by

$$\Delta E=IMwJ(y), \tag{8}$$

where

$$J(y)=G(y)+\tfrac{1}{2}h(y^2-1),$$
$$h=H/H_I,$$
$$H_I=I/2\pi w=\text{field due to current}. \tag{9}$$

$J(y)$ and, hence, ΔE vanish for

$$h=2G(y)/(1-y^2). \tag{10}$$

This simply expresses the condition that the formation of a sheath decreases the energy only if the applied field is small enough. For $\kappa<\frac{1}{2}$, $J(y)$ has both a maxi-

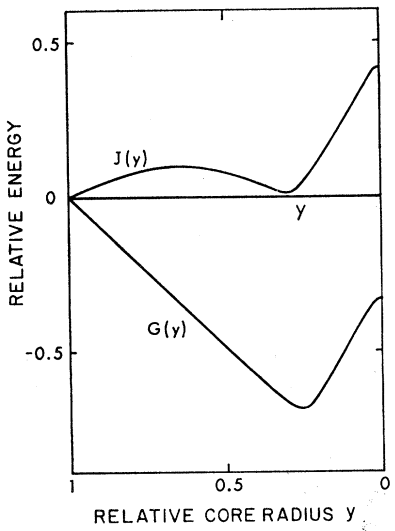

FIG. 15. Lower curve $G(y)$ shows energy-versus-core radius for a field-free sample. Upper curve $J(y)$ shows energy-versus-core radius for a sample in an applied magnetic field corresponding to $h=1.5$.

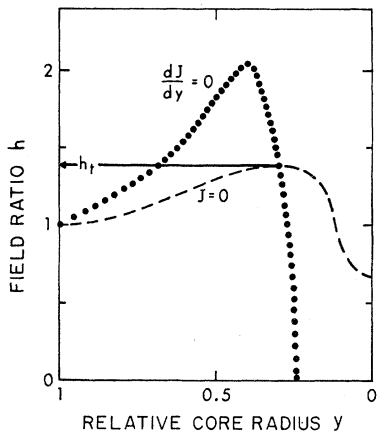

FIG. 16. Curves show the loci of extremal energy, $dJ/dy=0$, and of constant energy, $J=0$, in the h,y plane. The resistance transition occurs along the constant field line $h=h_t$.

mum and a minimum which occur simultaneously as shown in Fig. 15. These extrema are given by the equation

$$h=F(y)R^2(y). \tag{11}$$

For a sample in a small longitudinal magnetic field this relation plus the boundary condition $y=1$ can be regarded as equations of state for the system, since they represent all possible extrema of energy. The loci of the minima and the maxima in the h,y plane are shown by the solid and dotted lines, respectively, in Fig. 16. One can recognize here the familiar pattern of a first-order phase transition. Indeed, y is to be determined by the minimization of a potential function depending on h and κ, and both of these variables have critical values of $h>1$ and $\kappa<\frac{1}{2}$. These critical values give the conditions for the existence of two distinct states between which transitions can occur by discontinuous changes of y. For comparison to a more familiar case, y plays the role of the volume, h plays the role of the pressure, and κ plays the role of the temperature in a liquid-gas phase transition. These transitions occur at the values of h for which the minimum of $J(y)$ in Fig. 15 just crosses the abscissa, or where the minimum locus crosses the constant energy line $J(y)=0$ shown as the dashed line in Fig. 16 and following from the condition given by Eq. (10).

This analysis thus shows that as h decreases owing either to decrease of the longitudinal magnetic field or to increase of the current, the uniform longitudinal magnetization corresponding to $y=1$ will suddenly switch to a sheath-core configuration. This will then slowly evolve along the minimum line toward the spontaneous spin arrangement of the cylinder with no applied magnetic field. The predicted changes of resistance as a function h are represented in Fig. 17, where R is given by Eq. (3).

Extension of this theory to specimens with a square cross section and with easy directions of magnetization parallel to the surfaces is difficult since the solenoidal field induces demagnetizing effects dependent on the strength of the self-field of the current. Only the two cases of small and large currents can be examined easily.

For small currents, the spins remain parallel to the surfaces and the magnetic field remain solenoidal. The magnetic energy of the sheath can be calculated by taking into account the average cosine of the angle between field and magnetization which will be $2\sqrt{2}/\pi$ for the expected domain configuration shown in Fig. 11(b). If, in addition, the square cross section of side s is replaced by a circle of equal area, then the average value for the parameter h is given by

$$h=\frac{\pi H}{2\sqrt{2}}\frac{2\sqrt{\pi}s}{I}=\frac{H}{I}4s\times 0.986. \tag{12}$$

For very large currents, the self-field will be sufficient to rotate the spins away from easy directions. This will cause poles to form which will tend to align the total field with the magnetization. In this limit, energy relations identical to those of Eqs. (10) and (11) are obtained with h given by

$$h=(H/I)4s. \tag{13}$$

From consideration of the two limiting cases above, neither the geometry of the specimen nor demagnetizing effects would be expected to alter significantly the transition phenomenon, since the results for both small and large currents are nearly identical. Equation (13) will therefore be sufficiently accurate to treat the intermediate cases arising in practice.

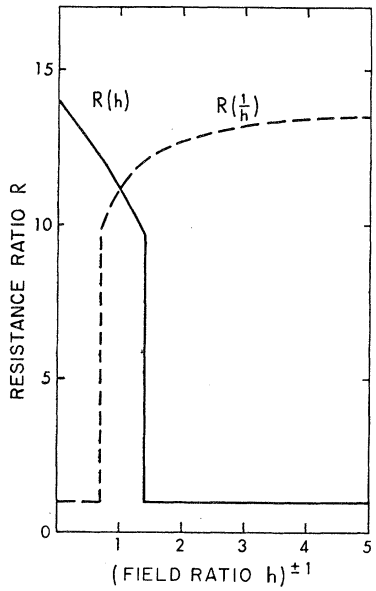

FIG. 17. Curves show predicted variations of resistance as a function of applied field, $R(h)$, or as a function of measuring current, $R(1/h)$.

Additional magnetic effects will, of course, be present and they can also be introduced into the analysis. For example, coercive forces will tend to hinder the motion of the sheath-core Bloch wall and this will tend to retard the development of the sheath as the current is increased. An equivalent coercive field $\mathbf{H}_C$ can be introduced into the definition of h in order to take into account coercive effects. The coercive effects also fluctuate randomly in space and this will tend to distort the wall and smear out the transition.

Magnetostrictive forces due to the application of longitudinal stress can also be taken into account. For the ⟨100⟩ specimens and positive λ_{100}, the core energy is lowered by application of a longitudinal stress while the sheath energy is invariant. If the stress is applied in the [100] direction then the magnetoelastic energy for the [100] direction will be $-\frac{3}{2}\lambda_{100}\sigma$ relative to the other two easy directions of magnetization, [010] and [001]. The value of the parameter h is then given by

$$h=H/H_I=[(H+H_c)M+\tfrac{3}{2}\lambda_{100}\sigma]4s/IM\,, \qquad (14)$$

where both the coercive force and the magnetoelastic energy have been taken into account. The critical current required for the transition in the presence of a longitudinal stress can therefore be written

$$I_c=(1/h_t)[(H+H_c)M+\tfrac{3}{2}\lambda_{100}\sigma]4s/M\,, \qquad (15)$$

where h_t is the h value for which the minimum of $J(y)$ crosses the abscissa (see Fig. 15) and a transition can occur. The critical current is therefore a linear function of the stress and the slope is given by

$$\frac{dI_c}{d\sigma}=\frac{6\lambda_{100}s}{Mh_t}. \qquad (16)$$

The h_t value will be a function of the value of $\kappa=\rho_L/\rho_T$ for the particular specimen being measured and can be deduced from a measurement of the resistance ratio R. The saturation magnetostriction constant can then be calculated from the expression

$$\lambda_{100}=\frac{Mh_t}{6s}\frac{dI_c}{d\sigma}. \qquad (17)$$

Experimentally, we observe rather smeared out resistance transitions as current and applied field are varied. However, the transition obtained in a number of samples by varying the current follows the theory rather well. A quasidiscontinuous change in resistance followed by a slower increase is indeed clearly visible in Fig. 14 and can be compared to the prediction of Fig. 17 (larger current corresponds to smaller h).

In samples where the observed change in resistance is a factor of 10 or more, the calculated transverse to longitudinal resistivity ratio is greater than 30. This means that the carriers dominating the conductivity have very long relaxation times in agreement with the transverse magnetoresistance observed at saturation.[1]

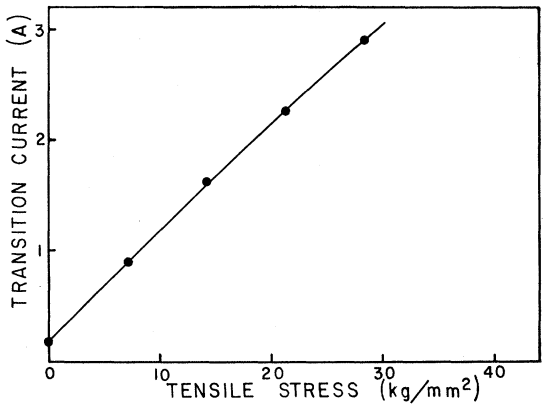

FIG. 18. Plot of the measured transition current as a function of stress. Experimental data are shown as solid circles.

We can use the resistance transitions observed in the stress experiments to determine the magnetostriction constant λ_{100}. If we consider the transition point as corresponding to the midpoint of the smeared steps in Fig. 14, then we find an approximately linear relationship between the transition current I_c and the applied stress σ as shown in Fig. 18. From the experimental curves of Fig. 14, the change in resistance ratio corresponding to the transition is estimated to be approximately 4. κ is therefore calculated to be about 1/7 and $h_t(\kappa)=1.14$. From Fig. 18, the initial slope is measured to be 0.103 ± 0.002 A mm²/kg. Using the values of $s=168\pm5\mu$ and $\mathbf{M}=21.8$ kG, Eq. (16) then gives a value of the magnetostriction constant of $\lambda_{100}=(25.0\pm1.0)\times10^{-6}$.

We have made measurements on a number of ⟨100⟩-axial specimens all having rather low values of the resistance change and exhibiting varying degrees of smearing in the resistance transition. An alternative method of calculating the value of λ_{100} is to take I_c from the point of initial nucleation of the sheath and assume that the initial sheath is very thin so that substantial current rearrangement in the specimen has not yet taken place. Using data from five samples this gives an average value of $(22.0\pm1.0)\times10^{-6}$ with agreement from specimen to specimen. This value is therefore in reasonable agreement with the value calculated from the accurate phase transition model above which was applied to the specimen showing the sharpest resistance transition.

Values of λ_{100} obtained in other experiments along with the present value obtained from the phase transition model are listed in Table I. The agreement is rather good and offers a reasonable check on the correctness of the model being used.

The actual mechanisms contributing to the magnetoresistance are, of course, still subject to interpretation, but at present it is assumed that the magnetoresistance

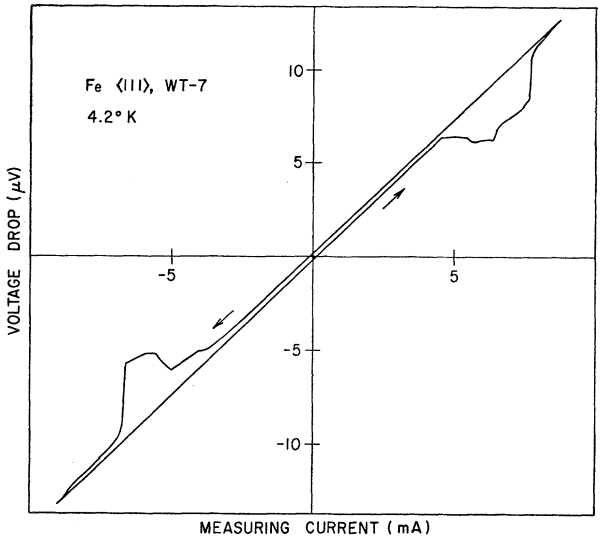

FIG. 19. Voltage drop as a function of measuring current for a ⟨111⟩-axial crystal. Hysteresis corresponding to domain reversal is observed.

is caused by the Lorentz force $\mathbf{v}\times\mathbf{B}$ on the electron and can be calculated from the conductivity tensor in a magnetic field.[16] The appropriate values of transverse and longitudinal magnetoresistance would be used to calculate the resistance of the sheath-core configuration in the above model.

The rotational domain structure induced by the measuring current and used to develop the above model for the ⟨100⟩-axial specimens has also been used by Tatsumoto[14] to successfully explain his measurements of magnetostriction at room temperature.

C. Magnetostriction and Magnetoresistance in ⟨111⟩ Whiskers

In the case of the ⟨111⟩-axial specimens, the application of stress produces an increase of resistance in all portions of the R-versus-$\mathbf{H}$ curve. Since two different regions of the R-versus-$\mathbf{H}$ curve have been identified in this case, it is useful to discuss the effect of stress on these regions separately. One of these is the spin-rotation region observed at higher fields and is simply interpreted as a decrease in the $\mathbf{v}\times\mathbf{B}$ terms of the resistivity as the spins are all rotated into a ⟨111⟩ direction and a pure longitudinal magnetoresistance is obtained. As seen in Fig. 10, the application of uniaxial stress increases the resistance at given field values in the rotation region and also extends the rotation region to slightly higher-field strengths. Both of these observations are consistent with the negative value of λ_{111} and indicate a spin rotation away from a ⟨111⟩ direction as a result of the stress. The amount of rotation induced by the maximum stress of 43 kg/mm² is estimated to be on the order of 5°–10°, which is sufficient to account for all of the resistance increase due to stress observed in the coherent spin-rotation region. The large anisotropy-energy increase for spin rotation away from ⟨100⟩ would also be expected to limit the rotation induced by stress.

TABLE I. Experimental data on magnetostriction in iron.

λ_{100} $\delta L/L$	Temp. °K	Expt
$(25.0\pm1.0)\times10^{-6}$	4.2	Present expt
23×10^{-6}	4.2	Gersdorf[a]
20×10^{-6}	4.2°K extrapolated from 77°K	Tatsumoto and Tetsuhiko[b]
25×10^{-6}	4.2°K extrapolated from 77°K	Williams and Pavlovic[c]

[a] See Ref. 13. [b] See Ref. 14. [c] See Ref. 15.

[16] E. Fawcett, Advan. Phys. 13, 139 (1964).

The sharp resistance peak observed at $\mathbf{M}\simeq0$ also increases with applied stress, the increase being somewhat larger than that observed for the coherent spin-rotation region. In fact, the stress-induced resistance continually increases as the applied longitudinal magnetic field is reduced to zero. The maximum resistance increase due to stress occurs at $\mathbf{M}\simeq0$, but this is also accounted for by a spin rotation of no more that 5°–10°.

The self-field of the current would also tend to rotate the spins into directions more perpendicular to the crystal axis. However, the above observations seem to indicate that such an effect is very small. In addition, the resistance at $\mathbf{M}\simeq0$ for the ⟨111⟩ specimens increases slowly with current up to the highest values measured (10 A), and this is consistent with a continually increasing small rotation of spins away from ⟨100⟩ directions. Since the initial six-domain zero-field configuration also provides a nearly solenoidal spin-rotation configuration, the self-field of the current would not be expected to produce extensive domain rearrangement at $\mathbf{M}\simeq0$. Reversal of the current would, however, be expected to reverse the sense of rotation, that is, clockwise to counterclockwise or vice versa. Structure in the voltage-versus-current curves for perfect ⟨111⟩ specimens indicates that this does occur, and an example is shown in Fig. 19. The structure shows hysteresis and occurs symmetrically on either side of zero current. After switching, the resistance returns to the same value with no current dependence of the resistance observable over the whole current range except during the switching process. The general conclusion from these results is that near $\mathbf{M}\simeq0$ the spins remain near the ⟨100⟩ directions and that the large extra resistance at $\mathbf{M}\simeq0$ is essentially current-independent and not accounted for by spin rotation as was the case for ⟨100⟩-axial specimens. In a number of the ⟨111⟩ specimens we have observed a current-induced resistance at $\mathbf{M}\simeq0$ which accounts for part but not all of the extra resistance at $\mathbf{M}\simeq0$. We now believe that this may show up in the whiskers with a less perfect

domain configuration and does not appear in the perfect case, as, for example, the specimen used to obtain Fig. 19. Suggested interpretations of the ⟨111⟩ behavior at $\mathbf{M}\simeq 0$ based on current-induced spin rotations and outlined in a previous paper[3] now appear to be ruled out.

The central resistance peak observed at $\mathbf{M}\simeq 0$ in ⟨111⟩ specimens must therefore be explained by some mechanism that depends on the detailed domain-wall arrangement and this must change significantly during low-field magnetization by domain-boundary motion. No spin reorientation relative to the current would occur during this process, in contrast to the ⟨100⟩ case. The most likely domain-configuration change producing a new magnetization along ⟨111⟩ is pictured in Fig. 12(b), where the three favorably oriented domains grow at the expense of the other three. Even if domain walls were good scattering centers, it is not obvious how the change from 6 to 3 walls parallel to the current could have such a large effect. Shifts in the domain walls might produce large anisotropics in the current flow, but a detailed model involving electron trajectories, mean free paths, and possible Fermi-surface effects would have to be developed. It is also possible that the intersection of (111) domain walls at the center of the specimen produces a complex core structure which plays some role in the scattering. Fivaz[17] has suggested that domain walls might be good reflectors of long mean-free-path electrons due to strong spin-orbit coupling effects and resulting Fermi-surface changes across the domain boundary.

IV. CONCLUSIONS

The stress experiments on ⟨100⟩-axial iron crystals have provided a clear interpretation of the low-field magnetoresistance behavior at liquid-helium temperatures. We have shown that the current-induced resistance peak observed for the flux-closed state can be quenched by inverse magnetostriction. This leads to a model of magnetoresistance behavior based on spin rotations which are induced by the self-field of the current or by the applied stress. The model involves a sheath-core configuration of the sample where spins are perpendicular to the current in the sheath and parallel to the current in the core. Analytical expressions have been derived for the resistance and these have been used to satisfactorily predict the observed resistance transitions in ⟨100⟩-axial specimens. In many respects, the behavior under favorable conditions simulates the behavior observed in a first-order phase transition. By including the applied stress field in the model we are able to obtain a value of the saturation magnetostriction constant λ_{100}. The value obtained is $(25.0\pm 1.0)\times 10^{-6}$.

In the case of ⟨111⟩-axial iron crystals, stress experiments have not allowed such a complete interpretation. The magnetostriction constant for the ⟨111⟩ direction is negative and this is consistent with the increase of magnetoresistance observed when stress is applied. This, however, rules out any balance between inverse magnetostriction and self-field effects that was effectively utilized for interpretation of the ⟨100⟩ behavior. The magnitude of the stress-induced increase of magnetoresistance in ⟨111⟩ specimens, however, allows us to estimate the amount of spin rotation occurring. We conclude that it is relatively small at flux closure when produced either by stress or by the self-field of the current. This implies that the extra resistance peak observed at flux closure in the ⟨111⟩-axial specimens is not connected with spin rotation. Therefore, the associated reverse galvanomagnetic effects that can be used to explain the ⟨100⟩-resistance peak do not apply in this case. An alternative source for this resistance peak is not clear at the present time. Previous suggestions such as domain-boundary scattering, Fermi-surface topology changes, or size effects could be playing a role, but definite evidence was not found in the present experiments. Further experiments will be required to resolve this point.

ACKNOWLEDGMENTS

The authors would like to acknowledge many valuable discussions with Dr. John E. Christopher and Dr. W. Trussel. The authors would also like to thank Dr. Acar Isin for use of his data on magnetization and derivatives of magnetization at helium temperatures. Phillip Sommer and Warner Frewer have made valuable contributions to the construction of the apparatus.

[17] R. C. Fivaz, Phys. Letters **30**, 72 (1969).

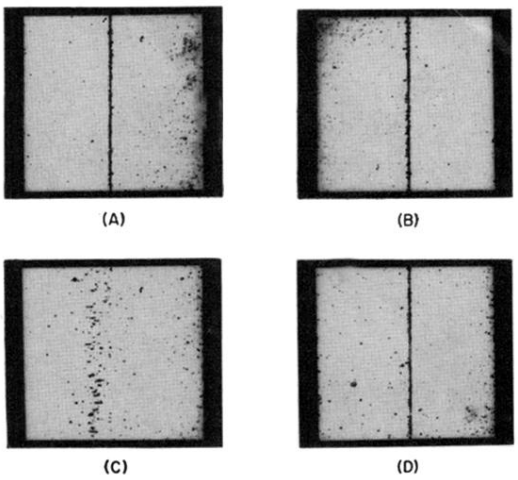

FIG. 10. Bitter-pattern photographs showing the annihilation and reformation of a longitudinal 180° Bloch wall caused by varying the longitudinal measuring current. (A) zero current, (B) and (C) current on, (D) zero current.